Article

A 1900 Year Sediment Record Suggests Recent Establishment of Black Mangrove (*Avicennia germinans*) Stands within a Salt Marsh in St. Augustine, Florida, USA

Jessica Chamberlin [1], Camryn Soehnlein [1], Jason Evans [1,2] and Benjamin Tanner [1,*]

1. Department of Environmental Science and Studies, Stetson University, DeLand, FL 32723, USA; jnchambe@stetson.edu (J.C.); camryn.soehnlein@state.co.us (C.S.); jevans1@stetson.edu (J.E.)
2. Institute for Water and Environmental Resilience, Stetson University, DeLand, FL 32723, USA
* Correspondence: btanner@stetson.edu; Tel.: +1-38-6822-7382

Abstract: Salt marshes and mangroves are currently being affected by rising temperatures. Mangroves thrive below −29° N latitude in Florida, USA, and have a low tolerance for extreme cold events, whereas salt marshes dominate further north. One potential effect of climate change is a reduction in the frequency of extreme cold events, which may lead to mangrove expansion into salt marsh systems. Our research identified sediment proxy indicators of salt marsh and mangrove environments. These indicators were applied to soil cores from intertidal wetlands near the current northern limit of mangrove presence on the east coast of Florida, to determine if mangrove expansion into salt marsh environments has precedence in the deeper past. Our findings suggest that mangrove and salt marsh sediments can be distinguished using a combination of stable carbon isotope ratios of sedimentary organic matter and macroscopic plant fragments, and our results showed that a mangrove stand that we cored established only recently. This result is consistent with other work in the southeastern United States that suggests that mangroves established at the current boreal limit only recently after the end of the Little Ice Age, and that the current mangrove expansion may be fueled by anthropogenic climate change.

Keywords: mangrove migration; climate change; Holocene; soil core; Florida; multi-proxy

1. Introduction

Current climate change, caused largely by anthropogenic increases in greenhouse gas concentration, is affecting Earth's temperatures, weather patterns, and ecosystems. Increasing levels of greenhouse gasses in the atmosphere have led to increases in global temperatures and decreases in extreme cold events [1]. These climate changes have resulted in impacts on different ecosystems and the services they provide.

Coastal saline wetlands in Florida, USA, contain a diverse mosaic of woody mangroves and herbaceous saltmarsh vegetative communities. On a global basis, mangrove communities tend to dominate in lower latitudes, generally below −29° N, while salt marshes dominate higher latitude settings [2]. Physiological tolerance to cold is a primary control on the position of the ecotone between mangroves and saltmarshes, with cold-intolerant mangrove communities largely being restricted to warmer, tropical, and sub-tropical latitudes [3,4]. At a local level, the mangrove/saltmarsh ecotone position may also result from elevation changes, hurricanes, increased predation, or rising sea levels [5–9]. Cavanaugh et al. [10] found that a temperature-related ecological threshold of −4 °C provides a control on mangrove distribution and favors stable-state dominance by herbaceous saltmarsh ecosystems in northern Florida. Osland et al. [11] found that while leaf damage occurs close to −4 °C for *Avicennia germinans* (black mangrove, the northern-most species in Florida), mortality occurs near −7 °C. However, Cavanaugh et al. [10] also found, through analysis of satellite imagery, substantial increases in mangrove area and the northward

incursion of mangrove distribution along the northeast coast of Florida over the past three decades. Mangrove expansion has also been documented along the west Florida coast and northern Gulf of Mexico [12]. This local mangrove expansion is consistent with more global work by Saintilan et al. [13], who provide evidence of mangrove expansion across at least five continents over the last half-century.

A logical inference from such observations is that decreases in the occurrence in killing frosts, as associated with anthropogenic climate warming, are favoring mangrove expansion in Florida and, more generally, across the subtropical world. The actual mechanism for mangrove expansion could be the decrease in the frequency of extreme cold events, which allows freeze-intolerant mangroves to expand [3]. However, it is also clear that periodic freezes result in the loss of mangrove communities, and that these communities may require decades to recover [12,14]. Because several historical freezes occurred in central and northern Florida in the 1980s, there is some question as to whether observed regional mangrove expansion since that time can, in fact, be cited as evidence of an anomalous long-term warming trend within the local and regional climate. A study conducted in Flagler County, FL, based on analysis of historical aerial photography and satellite imagery, showed multiple episodes of mangrove expansion between 1942 and 2013 [15]. A plausible alternative explanation is that the mangrove increases documented by Cavanaugh et al. [10] are simply an indicator of stochastic climate variability and, more specifically, a "rebound" from the impacts of a series of killing freezes. This line of reasoning is supported by further work, which has shown that mangrove expansion and contraction may have precedence in the deeper past, with historical records showing fluctuations in mangrove presence near its current northern limit in Florida due to a series of extreme cold events over the past 250 years [16]. There is currently only limited, but valuable, evidence that can be used to determine if the current regional mangrove expansion is anomalous in deeper time or if there is precedent for past ecotonal shifts before the period covered by aerial and satellite imagery or historical records [17,18].

Both mangrove and salt marsh communities are important in terms of their capacity to support commercial and sport fisheries, buffer storm surge, protect groundwater resources, mitigate sea-level rise, store carbon, and provide other services [19,20]. However, the biotic communities and specific ecosystem services are qualitatively different between the communities, and changes in the position of the ecotone will logically affect these services [21], including quantitative differences in carbon sequestration benefits [22]. For example, Vaughn et al. [22] found that sites in transition from salt marsh to mangrove receive increased soil accretion, carbon burial, and refractory carbon than comparable salt marsh sites, suggesting that they represent a more efficient carbon sink. Local agencies have committed to shoreline restoration as an optimal means to sustain these ecosystem services under conditions of urban expansion and sea-level rise. It is essential to know the historical context, including the likelihood of plant community survival and persistence with a changing climate, when setting restoration targets and goals [23].

The primary, guiding objective of this study was to elucidate past shifts of the salt marsh/mangrove ecotone over longer timescales in order to evaluate decadal- to centennial-scale variability. Intertidal wetlands, including salt marshes and mangroves, accumulate mineral and organic sediments that potentially reveal information about past environments [24–26]. Surface soil samples were collected from extant salt marsh and mangrove environments around the historic transition zone near Ponce Inlet, FL, and proxy indicators were employed to establish a fingerprint for each type of environment. These indicators were applied to a series of sediment cores recovered from near the current northern limit of significant black mangrove stands near St. Augustine, FL, in order to apply the proxy indicators to ancient sediment deposits and also begin to test for the presence of past mangrove deposits near the current northern limit. Measured proxy indicators also allowed for the determination of long-term carbon sequestration rates.

Previous research has shown that specific physical signatures, such as macroscopic core description, loss on ignition (LOI), and water content, along with chemical signatures

including carbon content, carbon isotope ratios, and carbon to nitrogen ratios, can be used to identify and fingerprint different intertidal wetland environments recorded in sediments [24–27]. Salt marshes are composed of plants utilizing either the C3, C4, or CAM photosynthetic pathways, whereas only C3 plants comprise mangroves [26]. The C4 plants are more water-efficient than C3 plants and fix more heavy carbon (^{13}C) during photosynthesis [28]. The large ($-12‰$) carbon isotopic difference between the plants operating under these different photosynthetic pathways can be used to help distinguish between C3 and C4 species dominance in a mixture of older sediments [29]. Sediment C/N is also used to help distinguish carbon sources, as this marker is especially sensitive to higher plant vs. algal contributions to sediments, although these values are affected by decomposition, with C/N settling to ratios between 10 and 20 through time [26]. We used a combination of these proxy measures (macroscopic core description, water content, bulk density, LOI, %C, C/N, and δ^{13}C) to fingerprint salt marsh vs. mangrove surface soils, because surface soil samples represent a "time average" of contributions to the sediments [26], and then applied the indicators to core deposits in order to interpret saltmarsh and mangrove fluctuations through time.

2. Materials and Methods

Surface soil samples were collected in May of 2017 at Ponce Preserve Park in the town of Ponce Inlet and at the Marine Discovery Center in New Smyrna Beach, Florida (see Figure 1). Both of these locations occur within the historic transition zone between salt marsh and mangrove environments and currently contain both ecosystem types. We took surface samples from *Spartina alterniflora* (Salt Marsh Cordgrass) dominated salt marshes at Ponce Inlet Park, where the marsh vegetation was extensive and mostly unmixed with mangroves, and mangrove surface samples from both Ponce Inlet Park and at the Marine Discovery Center, where there were extensive, well-developed mangrove systems dominated by black mangrove (see Supplementary). *Rhizophora mangle* (red mangrove) and *Laguncularia racemose* (white mangrove) were also present in minor abundance near the black mangrove surface sampling locations [30].

Three soil cores were removed from black mangrove stands in St. Augustine, Florida on 23 March 2018, using a half-spoon, 1 m length, and 4 cm diameter Eijkelkamp push corer. Boat reconnaissance along the Intracoastal Waterway north of St. Augustine revealed that our core sampling locations were at the northern limit of sizable mangrove-dominated stands in the area, although individual black mangroves and small clumps of black mangroves were found north of our coring locations, and other researchers have reported extant black mangrove stands as far north as Fort George Inlet, near Jacksonville, FL [16]. Two of the soil cores were taken at Nease Park near St. Augustine, Florida (29°55′35″ N, 81°17′51″ W) within a stand of black mangroves that was bounded on one side by *Spartina alterniflora* or *Batis maritima* (saltwort)—dominated salt marsh and on the other side by upland (Figure 1). Another core was taken within a black mangrove stand surrounded by *Spartina alterniflora*-dominated salt marsh near the Vilano Boat Ramp, St. Augustine (29°54′43″ N, 81°18′22″ W; Figure 1).

Surface soil samples from the Marine Discovery Center were collected from random points within the mangrove stands and were collected along transects at Ponce Preserve, through salt marsh and mangrove separately. A total of 30 surface samples were collected from mangrove stands, and an additional 30 samples were collected from the salt marsh by either sub-sampling from the top of shallow soil cores using a modified 1.5 cm diameter plastic syringe with volume indicators, or by using the plastic syringe to sample the surface sediments directly. In this way sampled sediment volume was recorded for later bulk density measurements. Surface samples were described in the field for Munsell color, texture (using the texture-by-feel method, [31]), and macroscopic sediment characteristics, such as the presence of woody versus grass fragments. Samples from each location were returned to the lab for further, immediate processing.
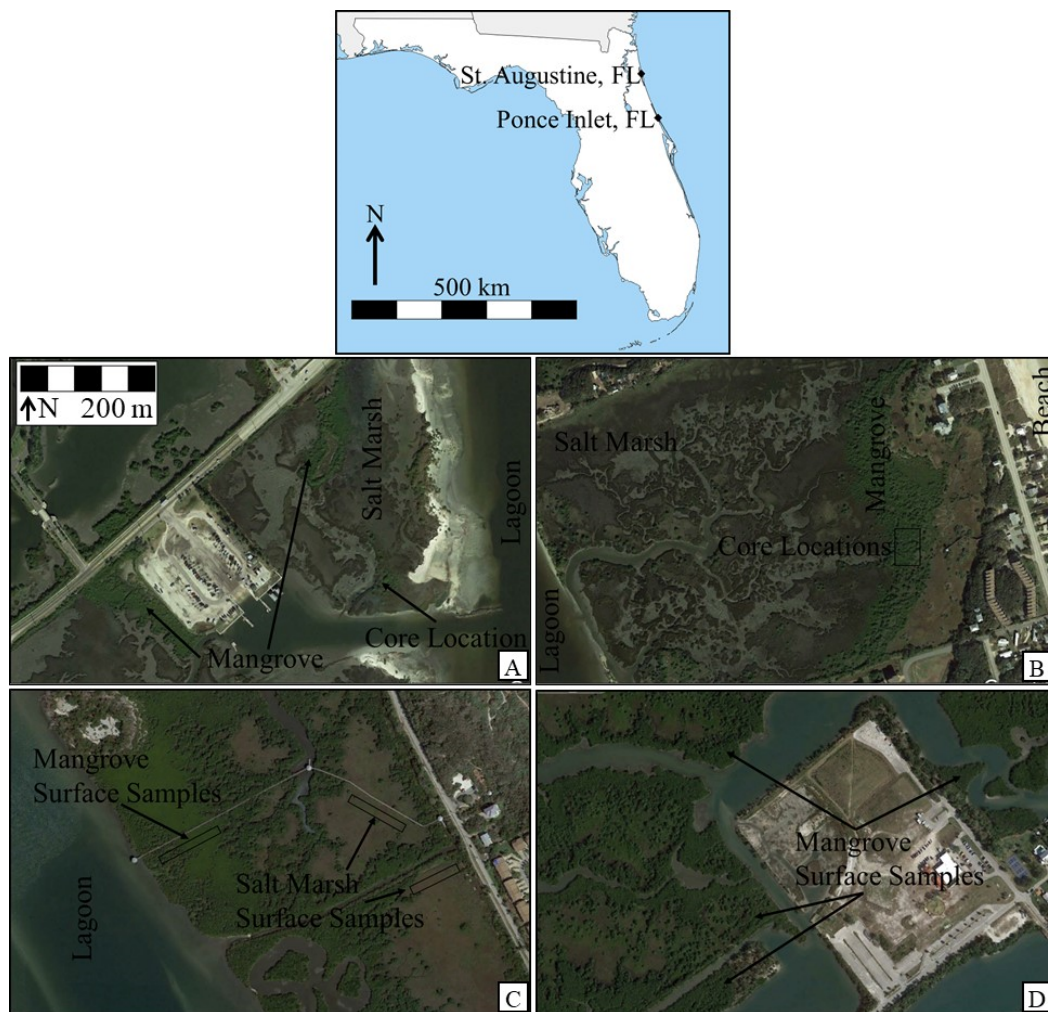
Figure 1. Base map of FL, USA (**Top**), and satellite images from Google Earth of the four field sites (**A**–**D**). The Vilano Boat Launch (**A**) and Nease Park (**B**) satellite images were taken in December 2018, and those core sites are located near St. Augustine. The Ponce Inlet Preserve (**C**) and Marine Discovery Center (**D**) satellite images were taken in March 2017 and those surface sample sites are located near Ponce Inlet.

The core samples were transported to the Environmental Science lab at Stetson University, where they were processed further. Modified plastic syringes were used to sub-sample the cores at 3.5 to 5 cm intervals based on total core length, with shorter cores having a tighter sub-sampling interval. Sub-sample volumes were recorded, and then samples were transferred to aluminum dishes and weighed. Samples were then dried to a constant weight at 65 °C. Dry weight was recorded, and bulk density was then calculated by dividing sample weight by volume. Samples were then powdered using a mortar and pestle. The samples were split, with half of the sediment fraction sent for bulk C, N, and δ^{13}C analysis and the other half retained for loss on ignition measurements. Surface samples were processed and split in the same way. Samples were measured for loss on ignition through combustion at 550 °C for 2 h.

Samples sent for bulk C, N, δ^{13}C, and also for radiocarbon analysis were processed and analyzed in a similar way as described in Tanner et al. [27] and as summarized again here. Powdered core samples were measured for total organic carbon, nitrogen, and carbon isotope composition (δ^{13}C) using a Costech Elemental Analyzer (Costech Analytical Technologies Inc., Valencia, CA, USA) coupled to a Thermo-Finnigan Delta+ XL Mass Spectrometer (Thermo Finnigan LLC, San Jose, CA, USA) at the University of Tennessee's

Department of Earth and Planetary Sciences Stable Isotope Laboratory. Powdered core samples were measured for total organic carbon, nitrogen, and carbon isotope composition (δ^{13}C) using a Costech Elemental Analyzer coupled to a Thermo Delta V Plus Mass Spectrometer (Thermo Scientific, Waltham, MA, USA) at the University of North Carolina Wilmington's Center for Marine Science Isotope Ratio Mass Spectrometry Core Facility. Carbonates were removed from both surface and core samples through HCl pretreatment prior to analysis. All δ^{13}C values were reported relative to the V-PDB standard.

Multiple samples from all three coring locations were sent to International Chemical Analysis for radiocarbon dating of the bulk peat. Indicated sample depths represent the mid-point of the sediment sections sent for analysis. Radiocarbon analysis was performed by following standard procedures for organic sediments, and the calibrations were calculated using CALIB Rev. 7.1.0 (Stuiver, Reimer, and Reimer, Belfast, UK) and the IntCal13 calibration database [32]. These standard procedures included examination of the samples and manual removal of contaminants like rootlets during the physical pretreatment. Additionally, samples underwent Acid–Alkali–Acid pretreatment, which included acid (HCl) treatment to remove acid soluble compounds and secondary carbonates, as well as a base (NaOH) treatment to remove humic acids, and a final acid treatment (HCl) to eliminate atmospheric CO_2. Linear interpolation was used to assign ages between the dated horizons, and the age/depth models were based on the mid-point of the sediment section used for radiocarbon analysis and the median, 2σ age in cal BP (present = 1950).

Carbon sequestration rates were determined for different core segments by multiplying the sedimentation rate of that core segment (determined through the radiocarbon dating) by the average carbon content for that segment and the average bulk density for that core segment. This was done only for core sections where the paleoenvironmental interpretation (either salt marsh or mangrove) was robust.

Microsoft Excel v. 2013 software with the data analysis tool pack (Microsoft Corporation, Redmond, WA, USA) was used to test for significant differences in independent variables (water content, loss on ignition, bulk density, carbon content, C/N, and δ^{13}C) between mangrove and salt marsh groups for the sampled surface sediments. The same software was also used to test for correlation between the measured variables using the coefficient of determination (r^2). We performed multiple t-tests (homoscedastic, two-tailed distribution) to determine significant differences in means of the measured variables between the two groups (marsh and mangrove) at a significance level of $\alpha = 0.01$. A Bonferroni Correction was applied to the alpha value as a conservative method to counteract the problem of multiple comparisons by dividing that value (0.01) by the number of variables tested (6). Therefore, a significance of $\alpha = 0.01$ was achieved by assessing each comparison at $\alpha = 0.0017$.

3. Results

Thirty surface samples were recovered from *Spartina alterniflora* (with minor *Batis maritima* and lesser abundance of other species) dominated salt marsh and 30 surface samples were also recovered from mangrove (black mangrove dominated with minor red mangrove and *Batis maritima* and lesser abundance of other species) at Ponce Inlet, FL. Texture-by-feel grain size analysis revealed clay-rich sediments in both salt marsh and mangrove environments. Macroscopic description of surface sediments showed that the deposits can be visually distinguished by the abundant presence of grass fragments in salt marsh sediments and the presence of woody material in mangrove sediments (Figure 2).

Figure 2. The top photograph (**a**) shows a soil core from a salt marsh site with abundant grass fragments. The bottom photograph (**b**) shows a soil core from a mangrove site with fibrous roots, sticks, and woody fragments. Both of these images include the sediment surface (right side of each).

The surface samples from the mangrove sites in Volusia County, Florida, contained primarily silty clay (30% of samples), silty loam (27%), sandy clay (17%), and clay (13%) and consisted of fibrous roots, sticks and woody fragments (Figure 2). The surface samples from the salt marsh sites contained primarily silty clay (47% of samples), clay (33%), and silty loam (10%). The soil cores from St. Augustine, Florida, had similar texture and plant fragment content to the surface samples (Figure 3). In all three soil cores, woody fragments were noted in the upper sections of the cores and only grass fragments were found down the core.

Table 1 shows values for measured surface sediment physical and chemical characteristics, including water content, loss on ignition, bulk density, percent carbon, C/N, and $\delta^{13}C$ of organic matter. Compared to mangrove surface sediments, salt marsh surface sediments had a significantly higher ($p < 0.01$) water content (average 79.3% to 58.6%), loss on ignition (average 42.2% to 24.6%), carbon percentage (average 20.2% to 10.5%) and $\delta^{13}C$ value (average −19.3‰ to −23.91‰). Conversely, mangrove sediments showed a significantly higher ($p < 0.01$) bulk density (average 0.55 g/cm^3 to 0.23 g/cm^3). C/N showed no significant difference between salt marsh and mangrove surface sediments ($p = 0.14$). Loss on ignition values and percent carbon values were highly correlated ($r^2 = 0.67$), as would be expected (Table 2). Therefore, the percent carbon values are presented in Figure 3 without the loss on ignition values in order to avoid redundancy and to save space. Those measurements were also correlated with soil water content and bulk density (Table 2), as would be expected. Soils with a higher carbon content had a higher loss on ignition, higher water content, and lower bulk density. Black mangrove surface sediment samples showed a range of $\delta^{13}C$ values between −27.5‰ to −19.4‰ and *Spartina alterniflora* salt marsh surface sediment samples ranged from −24.9‰ to −14.0‰. Thus, *Spartina alterniflora*-dominated salt marsh and black mangrove-dominated surface samples had overlapping values between −24.9‰ to −19.4‰ (hence the vertical lines indicating mangrove, mixed, and salt marsh fields in Figure 3 related to the $\delta^{13}C$ values).
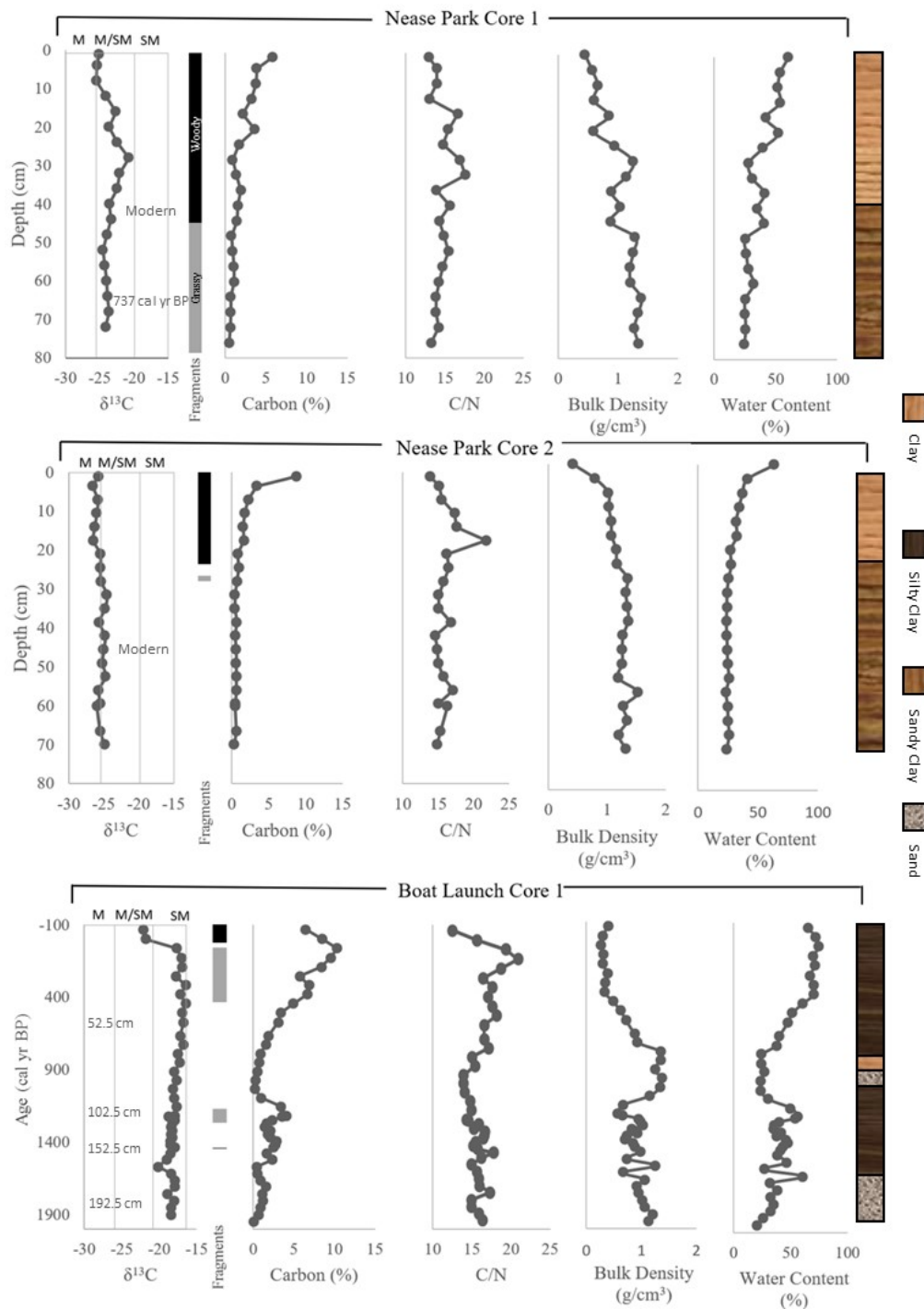
Figure 3. Measured variables (δ^{13}C, Carbon Content, C/N ratios, Bulk Density, and Water Content) are presented versus depth for the Nease Park cores and versus age for the Vilano Boat Launch core, where multiple radiocarbon dates allowed development of an age-depth model (negative ages are possible because present = 1950 by convention). The δ^{13}C plots include vertical lines indicating δ^{13}C values that were only found for mangrove (M) surface samples, salt marsh (SM) surface samples, and the range of overlapping values (M/SM) derived from analysis of surface samples. Presence of identifiable macroscopic fragments from the core description is indicated by black (mangrove woody fragments) and gray (salt marsh grass fragments) bars. Sediment texture for corresponding depth or age is also indicated. Median radiocarbon ages (and modern dates) are indicated at the correct sample depth for both Nease Park cores and sample depths are indicated for the Vilano Boat Launch core where radiocarbon ages were obtained.

Table 1. Surface sample percent water content, percent loss on ignition (LOI), percent carbon content, C/N ratio, and δ^{13}C values are presented for salt marsh and mangrove surface sediment samples along with mean values, standard deviations, and significance values (*p*) for differences between salt marsh and mangrove samples (from *t*-tests). Mangrove C/N was not significantly different than salt marsh C/N, but all other variables were significantly different (*p* < 0.01). A Bonferroni Correction was used to counteract the problem of multiple comparisons (see methods).

| Mangrove Samples | | | | | | | Salt Marsh Samples | | | | |
Water (%)	LOI (%)	Density (g/cm³)	C (%)	C/N	δ^{13}C (‰)		Water (%)	LOI (%)	Density (g/cm³)	C (%)	C/N
32.3	4.8	1.06	1.2	9.63	−20.06		78.5	36.4	0.22	14.3	13.48
32.3	6.4	1.06	1.1	9.53	−21.02		75.9	35.9	0.26	19.1	13.37
33.1	5.9	1.04	7.7	11.72	−20.72		76.7	34.4	0.27	16.8	13.47
51.1	16.5	0.67	10.1	12.31	−21.13		76.7	40.0	0.26	22.5	13.73
32.7	6.2	1.08	7.0	13.36	−21.14		79.0	35.8	0.22	20.5	13.19
51.7	27.9	0.79	4.3	11.16	−20.20		78.4	36.9	0.23	25.6	15.85
45.4	10.4	0.79	21.3	14.60	−20.63		78.6	37.1	0.23	19.8	12.69
51.8	11.3	0.76	4.3	13.16	−22.06		77.5	40.3	0.25	16.3	13.77
79.8	45.4	0.24	4.3	13.29	−21.15		77.8	45.3	0.23	14.5	11.64
29.5	3.7	1.07	4.5	12.94	−21.89		79.2	39.5	0.26	17.5	13.77
52.8	16.7	0.59	1.9	11.58	−20.37		79.7	38.3	0.22	16.2	12.81
55.0	21.6	0.55	6.3	14.05	−21.19		79.4	34.1	0.22	16.7	12.48
59.3	23.6	0.50	9.2	11.36	−19.40		81.1	40.9	0.20	15.5	11.76
52.5	15.2	0.63	4.9	11.29	−20.60		79.3	41.7	0.22	17.8	12.77
72.5	37.5	0.31	28.5	14.07	−21.26		79.1	39.6	0.22	25.2	17.79
55.6	14.9	0.57	1.9	12.75	−25.95		67.6	23.4	0.38	7.3	11.96
61.3	18.3	0.47	4.7	15.33	−26.67		68.7	28.3	0.36	10.3	11.16
41.5	6.8	0.83	1.7	13.68	−26.70		70.3	27.8	0.32	2.9	3.40
61.7	15.2	0.45	6.1	16.77	−26.61		70.3	26.4	0.34	21.5	12.09
73.0	33.3	0.32	11.3	15.06	−27.04		76.7	40.7	0.29	16.2	12.48
63.3	21.6	0.45	4.9	14.49	−26.63		79.6	44.5	0.22	18.2	12.83
74.2	37.2	0.28	16.1	15.14	−27.12		83.2	51.1	0.17	20.7	13.58
72.9	33.3	0.30	15.9	16.01	−27.31		83.0	56.3	0.19	23.6	13.65
72.1	42.9	0.29	17.6	15.83	−26.93		84.9	55.2	0.17	27.9	13.76
73.2	39.7	0.29	18.1	16.23	−27.03		84.7	55.9	0.17	30.9	14.26
74.8	37.8	0.27	18.5	15.28	−27.53		84.6	59.5	0.17	31.1	14.68
76.2	43.8	0.25	20.2	15.64	−27.23		85.9	50.9	0.16	29.3	13.85
76.0	51.4	0.25	23.1	17.86	−27.13		84.8	57.5	0.16	29.8	14.38
75.4	46.6	0.25	18.7	16.99	−27.20		84.2	58.8	0.17	31.7	13.71
76.3	41.2	0.24	20.8	16.34	−27.32		94.3	53.9	0.16	26.1	13.74
58.6	**24.6**	**0.55**	**10.5**	**13.92**	**−23.91**	**Mean**	**79.3**	**42.2**	**0.23**	**20.2**	**13.07**
16.0	**15.0**	**0.3**	**7.9**	**2.2**	**3.2**	**Std. Dev.**	**5.6**	**10.2**	**0.1**	**7.1**	**2.2**
<0.01	**<0.01**	**<0.01**	**<0.01**	**0.14**	**<0.01**	***p*=**	**<0.01**	**<0.01**	**<0.01**	**<0.01**	**0.14**

Table 2. Correlation matrix (r^2 values) for all of the measured surface sample variables (mangrove and salt marsh combined) including water content, loss on ignition (LOI), bulk density, percent carbon, and δ^{13}C.

	Water Content	LOI	Bulk Density	Percent Carbon	C/N	δ^{13}C
Water Content	NA	0.85	0.97	0.55	0.10	0.01
LOI	0.85	NA	0.79	0.67	0.11	0.00
Bulk Density	0.97	0.79	NA	0.49	0.11	0.00
Percent Carbon	0.55	0.67	0.49	NA	0.21	0.03
C/N	0.10	0.11	0.11	0.21	NA	0.11
δ^{13}C	0.01	0.00	0.00	0.03	0.11	NA

The soil cores from Nease Park were collected to refusal at 76 cm depth (core 1) and 70 cm depth (core 2). The soil core from the Vilano Boat Launch was collected to refusal at 205 cm depth. Radiocarbon ages for all cores are presented in Table 3 along with supporting information. The upper sample from Nease Park, core 1, and the sole sample from core 2 both returned modern ages. The deeper 66.5 cm sample depth from core 2 returned a median age of 737 cal BP. We did not attempt to date a deeper sample from core 2 because of a lack of datable organic material. Given that only one sample returned an age across both Nease Park cores, an age/depth model was not attempted, and all data are presented vs. depth for that site. Four radiocarbon ages were obtained for the Vilano Boat Launch core due to its greater length. All radiocarbon ages for the Vilano core were in stratigraphic order, and the median ages ranged from 604 cal BP at 52.5 cm depth to 1828 cal BP at 192 cm (Table 3). An age/depth model for that core was constructed using linear interpolation (Figure 4), and the age depth model was applied to the proxy data from the core (Figure 3). For the linear interpolation, the surface sample (1 cm) was assumed to represent the time of core collection (−78 cal BP).
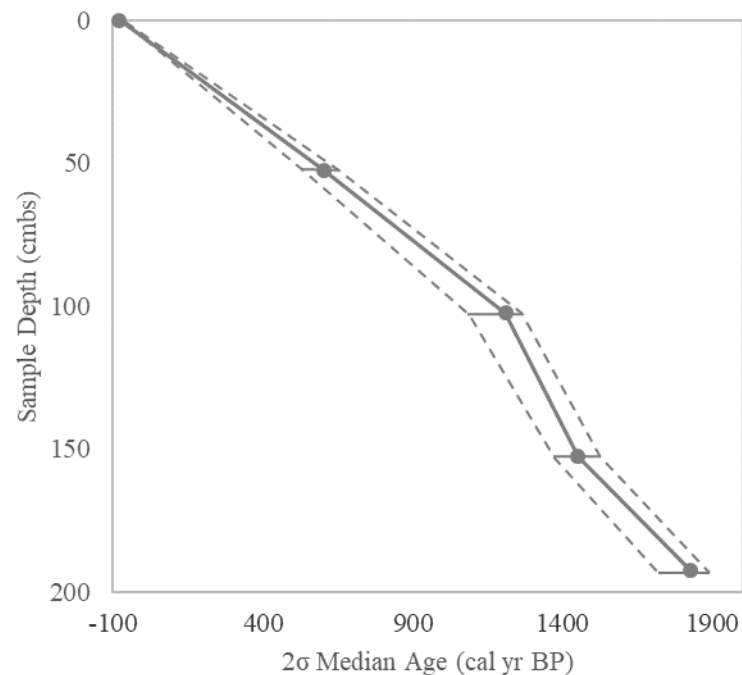
Table 3. Radiocarbon data are presented for the three cores. Sample depths are in cm below the ground surface and represent the mid-point of the sediment section sent for dating. The calibration procedures are described in the methods section.

Core/Depth	Conventional Radiocarbon Age (yrs BP)	Calibrated 2σ Range (cal yr BP)	Calibrated 2σ Range Median (cal yr BP)	Dated Material	Laboratory #
Nease Park Core 1					
42.5cm	Modern	NA	NA	Bulk Sediment	ICA-18OS/0449
66.5cm	830 ± 30	688 to 789	737	Bulk Sediment	ICA-18OS/0451
Nease Park Core 2					
46.5cm	Modern	NA	NA	Bulk Sediment	ICA-18OS/0448
Boat Launch Core					
52.5cm	580 ± 30	533 to 569 582 to 649	604	Bulk Sediment	ICA-18OS/0447
102.5cm	1240 ± 20	1082 to 1160 1172 to 1194 1196 to 1263	1211	Bulk Sediment	ICA-18OS/0446
152.5 cm	1540 ± 30	1365 to 1524	1451	Bulk Sediment	ICA-18OS/0450
192.5 cm	1880 ± 30	1729 to 1884	1828	Bulk Sediment	ICA-18OS/0452

The soil cores from Nease Park and the Vilano Boat Launch all showed a general decrease in organic carbon content and water content with depth, while bulk density generally increased with depth (Figure 3), as would be expected with temporal decomposition and compaction of organic matter. C/N varied between 12.5 and 21.8 among the three soil cores, showing no clear trends. The $\delta^{13}C$ values were almost all in the range of overlap between mangrove and salt marsh sediments for both Nease Park cores. For the Vilano Boat Launch core, $\delta^{13}C$ values were lower just at the surface (within the range of overlapping mangrove and salt marsh sediment values) and were higher with depth (in the range of salt marsh sediment values), in line with the trend of woody and grassy fragments recorded for that core.

The data from the well-dated Vilano Boat Launch core allowed for the calculation of carbon sequestration rates for both the mangrove-dominated upper sediments and the remainder of the core, dominated by salt marsh (Table 4). Data were divided into sections representing interpreted mangrove vs. salt marsh deposition (based on Figure 3) and then by differences in sedimentation rate between bracketed radiocarbon ages (see Table 3). Carbon sequestration rates were generally similar between the upper mangrove sediments (average = 20.01 g C m^{-2} yr^{-1}) and the underlying, older salt marsh sediments

(total average for all depth intervals = 21.53 g C m^{-2} yr^{-1}), with a relatively persistent sequestration rate over long time periods.

Figure 4. The radiocarbon age/depth curve is plotted for the Vilano Boat Launch core, where multiple radiocarbon dates were obtained. The data points represent the mid-point of the sample interval sent for radiocarbon age determination and the calibrated, 2σ median age in cal BP. The solid line connecting the points represents the linear interpolation between dated horizons. The dashed lines indicate the calibrated 2σ age ranges for the radiocarbon ages. The surface sample is assigned an age of −78 cal yr BP given that the samples were collected in 2018 and present equals 1950 by convention.

Table 4. Carbon sequestration data for the Vilano Boat Launch core are presented for depth intervals based on interpreted wetland environment (mangrove vs. salt marsh) and by differences in sedimentation rate between bracketed radiocarbon ages. The presented carbon percentages, sedimentation rates, and bulk densities represent averages for those sample depth intervals.

Depth Interval (cm)	Environmental Interpretation	Carbon Sequestration Rate (g C m^{-2} yr^{-1})	Carbon (%)	Sedimentation Rate (mm/yr)	Bulk Density (g/cm^3)
0 to 10	Mangrove	20.01	7.49	0.77	0.35
10 to 52.5	Salt Marsh	20.99	6.54	0.77	0.42
52.5 to 102.5	Salt Marsh	12.92	1.45	0.82	1.09
102.5 to 152.5	Salt Marsh	38.78	2.26	1.99	0.86
152 to 192.5	Salt Marsh	13.43	1.22	1.06	1.04

4. Discussion

Surface sediment samples collected from salt marsh and mangrove environments showed significant differences ($p < 0.01$) in water content, loss on ignition, bulk density, carbon percentage, and δ^{13}C (Table 1). In addition, salt marsh surface sediments contained abundant grassy fragments, whereas mangrove surface sediments contained woody material (Figure 2). Therefore, water content, loss on ignition, bulk density, carbon percentage, and δ^{13}C all have potential as proxy indicators to distinguish between salt marsh and mangrove sediments in core deposits, and several of these indicators have been used in other locations in this regard [17,18,33]. Our data suggest that C/N is not a metric

that is useful to distinguish between salt marsh and mangrove sediments for our study site (Table 1; *p* = 0.14), although others working in the region have found that mangrove deposits have a lower C/N, possibly due to additional algal inputs related to increased tidal inundation [22]. Recorded sediment textures were similar between salt marsh and mangrove surface sample sites, suggesting that soil texture cannot be effectively applied to core samples to distinguish salt marsh and mangrove environments for our study sites.

Of the measured proxy indicators that were potentially useful to distinguish salt marsh from mangrove sediments (water content, loss on ignition, bulk density, carbon percentage, δ^{13}C, and plant fragments), four logically change with depth. Loss on ignition and carbon percentages relate to soil bulk density and tend to decline with depth due to decomposition and soil compaction [34]. Our data showed that water content and bulk density are strongly correlated (Table 2) with an inverse relationship (data from Table 1). Declines of organic carbon and bulk density with depth and increases in water content with depth were seen in our core samples (Figure 3). Given that these four potential proxies were strongly related to depth down the soil profile as opposed to marsh vs. mangrove sediment input, they have limited utility in allowing discrimination between salt marsh and mangrove sediments in core deposits. Therefore, the best proxy indicators that we employed for distinguishing mangrove and salt marsh deposits included a combination of δ^{13}C values of sedimentary organic matter and plant fragment information.

Radiocarbon age determinations were obtained for bulk sediments for the Nease Park and Vilano Boat Launch cores. Plant macrofossils represent an ideal material used for radiocarbon dating because their carbon source is known and does not represent an admixture of multiple carbon sources [35]. However, we were not able to identify above-ground mangrove plant macrofossils that would be suitable for radiocarbon dating in the sediments. Only woody material was found in the sediments, which could have represented either above-ground timber or below-ground roots that are not suitable for radiocarbon age control [36]. Salt marsh grass fragments identified in the sediment deposits were fragile and we were not able to recover them intact. Bulk sediment is commonly used for radiocarbon chronologies in mangrove sediments [33,36]. Studies have shown that organic matter in both mangrove and salt marsh sediments is generally reflective of autochthonous sources [22,36–39]. In mangrove environments, the primary carbon source to the sediments is often represented by the mangrove plants themselves, followed by macro- and micro-algae, and finally transport and deposition from upstream materials and materials from the adjacent coastal zone [37]. A consistent age-depth model for the Vilano Boat Launch core with in-sequence radiocarbon ages (Figure 4) and reasonable calculated sedimentation rates (Table 4) suggested that the bulk radiocarbon ages for that core were robust and reflective of true ages of deposition for that core.

The two soil cores from Nease Park were relatively short (each <80 cm long), and only one non-modern radiocarbon age was returned, representing the deeper sediment sample from core 2 (Table 3). The lack of non-modern radiocarbon ages confounded the development of age/depth models for core 2. However, plant fragment data indicated the presence of a mangrove environment underlain by salt marsh deposits for both cores (Figure 3). Carbon isotope data for these two cores were ambiguous, however, as δ^{13}C values for both cores were mostly in the field of overlapping salt marsh and mangrove values, albeit towards the mangrove side of the overlapping range for both cores, and especially for core 2. The paleoenvironmental interpretation was therefore difficult for both of the Nease Park cores, given that plant fragment information suggested a mangrove to salt marsh transition for each core with depth, whereas δ^{13}C values were more suggestive of a persistent mangrove environment (or at the very least, a mixed salt marsh and mangrove environment) for both cores.

The interpretation of the Vilano Boat Launch core was facilitated by proxy indicators that were in good agreement (Figure 3). Also, all four radiocarbon dates obtained for the core were in stratigraphic order, and the age/depth model obtained through linear interpolation suggested a relatively constant sedimentation rate for the past −1900 cal BP at the

core location (Figure 4), without any obvious depositional hiatuses. The core was collected within a black mangrove stand that was surrounded by Spartina alterniflora-dominated salt marsh. The upper part of the core reflected deposition in a mangrove environment, with woody fragments and lower δ^{13}C values observed in sediments representing the past 100+ years (Figure 3). Only grass fragments were found deeper in the core, and the shift to higher δ^{13}C values for the remainder of the core, which were all in the range of C4 plant-dominated Spartina alterniflora salt marsh [24], suggested insignificant input from mangroves to the sediment pool for the remainder of the core. It was thus apparent that this core sampling location transitioned to mangrove only recently, after almost 1800 years of salt marsh deposition. It should be noted that coarse sediments (sand-dominated) were observed towards the middle and bottom parts of the core (Figure 3), indicating higher-energy deposition. This was perhaps due to closer proximity of a migrating tidal channel to the core site during times of coarse sediment deposition, or perhaps deposition from a high-energy event like a tropical cyclone, which would both increase the coarse sediment fraction and the deposition rate [40]. If the coarse sediment fraction was driven by a rapid event, such as a tropical, a high sedimentation rate for that depth interval would be expected. However, the sedimentation rate for the Vilano Boat Launch core was not highest where the sand layers were present and was instead higher in between the sand layers (Figure 3, Table 4).

The results from the well-dated Vilano Boat Launch core suggested a persistent salt marsh environment from approximately 1900 cal BP to approximately 50 cal BP, when significant mangrove sedimentation was then indicated to the present. A nearby study based on historical records and a climate-related "mangrove suitability" index suggested that mangrove stands were present in the region at least as far back as 1860 AD [16]. Our results do not contradict this record given the uncertainties inherent in radiocarbon dating and in the development of age/depth models. Our results were also consistent with research from coastal Louisiana, where researchers suggested the development of mangrove stands at the current boreal limit only after the Little Ice Age, ending between 1850 and 1890 AD [17].

Our data allowed for the calculation of carbon sequestration rates for the Vilano Boat Launch core (Table 4). These measured rates were similar to those reported from a nearby site for mangrove sediments and were higher than those reported for nearby salt marsh sediments [22]. They were lower by about one order of magnitude than average global rates of carbon storage for both salt marsh (218 ± 24 g C m^{-2} yr^{-1}) and mangrove (226 ± 31 g C m^{-2} yr^{-1}) systems, although there is considerable variability in carbon storage measurements across the globe [41]. Our carbon sequestration rate results, although limited, suggested that ecosystem services related to the efficiency of carbon burial are similar between salt marsh and mangrove systems in the area of our study over longer time periods (decadal to century scale). The higher percentage of carbon measured for the mangrove-dominated sediment was offset by the higher bulk density measured for the salt marsh sediments. Vaughn et al. [22] suggested that recalcitrant lignin associated with woody mangrove sediments allows for the potential for higher long-term carbon sequestration rates given slower potential decomposition. Our data suggest that salt marsh sediments can also store carbon efficiently over longer timescales in the region of our study.

5. Conclusions

Our results from surficial sediments suggest that mangrove sediments in northern Florida can be distinguished from C4 plant-dominated salt marsh sediments using a combination of stable carbon isotope ratios of sedimentary organic matter combined with macroscopic plant fragment material (woody vs. grassy). These indicators were applied to three soil cores recovered from near the modern black mangrove boreal limit in northern Florida, from within stands of black mangrove. Paleoenvironmental interpretation for two of the soil cores (from Nease Park) was ambiguous, and the short sediment record preserved at that site confounded the development of an age/depth model. The paleoenvironmental

proxy record developed from a core from the other site (Vilano Boat Launch) suggested C4 plant-dominated salt marsh deposition from the bottom of the core to around 50 cal BP, where there was a transition to mangrove-dominated sediments that persisted to the present time. This finding was consistent with work by others that suggests mangrove presence at its current boreal limit in the southeastern United States only within the past several hundred years and is also consistent with the hypothesis that the current observed mangrove expansion in the region is due to anthropogenic climate change.

Supplementary Materials: The following are available online at https://www.mdpi.com/article/10.3390/quat5010002/s1, Figure S1: photograph taken at Ponce Preserve Park showing mangrove and salt marsh, Figure S2: photograph of core collection at Nease Park, Figure S3: photograph of Vilano Boat Launch core showing sampling scheme.

Author Contributions: B.T. and J.E. conceptualized the study and were also involved with the study methodology, formal analysis, investigation, writing—original draft preparation, writing—review and editing, project administration, and funding acquisition. J.C. and C.S. conducted formal analysis, investigation, writing—original draft preparation, and writing—review and editing. All authors have read and agreed to the published version of the manuscript.

Conflicts of Interest: The authors declare no conflict of interest.

References

1. IPCC. *Climate Change 2021: The Physical Science Basis. Contribution of Working Group I to the Sixth Assessment Report of the Intergovernmental Panel on Climate Change*; Masson-Delmotte, V., Zhai, P., Pirani, A., Connors, S.L., Péan, C., Berger, S., Caud, N., Chen, Y., Goldfarb, L., Gomis, M.I., et al., Eds.; Cambridge University Press: Cambridge, UK, 2021. Available online: https://www.ipcc.ch/report/ar6/wg1/downloads/report/IPCC_AR6_WGI_SPM.pdf (accessed on 20 September 2021).
2. Mitsch, W.J.; Bernal, B.; Hernandez, M.E. Ecosystem Services of Wetlands. *Int. J. Biodivers. Sci. Ecosyst. Serv. Manag.* **2015**, *11*, 1–4. [CrossRef]
3. Stuart, S.A.; Choat, B.; Martin, K.C.; Holbrook, N.M.; Ball, M.C. The Role of Freezing in Setting the Latitudinal Limits of Mangrove Forests. *New Phytol.* **2007**, *173*, 576–583. [CrossRef]
4. Pickens, C.N.; Hester, M.W. Temperature Tolerance of Early Life History Stages of Black Mangrove Avicennia germinans: Implications for Range Expansion. *Estuaries Coasts* **2011**, *34*, 824–830. [CrossRef]
5. Doyle, T.W.; Smith, T.J.; Robblee, M.B. Wind Damage Effects of Hurricane Andrew on Mangrove Communities along the Southwest Coast of Florida, USA. *J. Coast. Res.* **1995**, *21*, 159–168. Available online: https://pubs.er.usgs.gov/publication/1008428 (accessed on 20 September 2021).
6. Kennedy, J.P.; Dangremond, E.M.; Hayes, M.A.; Preziosi, R.F.; Rowntree, J.K.; Feller, I.C. Hurricanes Overcome Migration Lag and Shape Intraspecific Genetic Variation Beyond a Poleward Mangrove Range Limit. *Mol. Ecol.* **2020**, *29*, 2583–2597. [CrossRef] [PubMed]
7. Langston, A.; Kaplan, D.; Angelini, C. Predation Restricts Black Mangrove (Avicennia germinans) Colonization at its Northern Range Limit along Florida's Gulf Coast. *Hydrobiologia* **2017**, *803*, 317–331. [CrossRef]
8. Leong, R.C.; Friess, D.A.; Crase, B.; Lee, W.K.; Webb, E.L. High-Resolution Pattern of Mangrove Species Distribution is Controlled by Surface Elevation. *Estuar. Coast. Shelf Sci.* **2018**, *202*, 185–192. [CrossRef]
9. Riascos, J.M.; Cantera, J.R.; Blanco-Liberos, J.F. Growth and Mortality of Mangrove Seedlings in the Wettest Neotropical Mangrove Forests during ENSO: Implications for Vulnerability to Climate Change. *Aquat. Bot.* **2018**, *147*, 34–42. [CrossRef]
10. Cavanaugh, K.C.; Kellner, J.R.; Forde, A.J.; Gruner, D.S.; Parker, J.D.; Rodriguez, W.; Feller, I.C. Poleward Expansion of Mangroves is a Threshold Response to Decreased Frequency of Extreme Cold Events. *Proc. Natl. Acad. Sci. USA* **2018**, *111*, 723–727. [CrossRef]
11. Osland, M.J.; Day, R.H.; Hall, C.T.; Feher, L.C.; Armitage, A.R.; Cebrian, J.; Dutton, K.H.; Hughes, A.R.; Kaplan, D.A.; Langston, A.K. Temperature Thresholds for Black Mangrove (Avicennia germinans) Freeze Damage, Mortality and Recovery in North America: Refining Tipping Points for Range Expansion in a Warming Climate. *J. Ecol.* **2020**, *108*, 654–665. [CrossRef]
12. Giri, C.; Long, J. Is the Geographic Range of Mangrove Forests in the Conterminous United States Really Expanding? *Sensors* **2016**, *16*, 2010. [CrossRef] [PubMed]
13. Saintilan, N.; Wilson, N.; Rogers, K.; Rajkaran, A.; Krauss, K.W. Mangrove Expansion and Salt Marsh Decline at Mangrove Poleward Limits. *Glob. Chang. Biol.* **2014**, *20*, 147–157. [CrossRef] [PubMed]
14. Stevens, P.; Fox, S.; Montague, C. The Interplay between Mangroves and Saltmarshes at the Transition between Temperate and Subtropical Climate in Florida. *Wetl. Ecol. Manag.* **2006**, *14*, 435–444. [CrossRef]

15. Rodriguez, W.; Feller, I.C.; Cavanaugh, K.C. Spatio-Temporal Changes of a Mangrove-Saltmarsh Ecotone in the Northeastern Coast of Florida, USA. *Glob. Ecol. Conserv.* **2016**, *7*, 245–261. [CrossRef]

16. Cavanaugh, K.C.; Dangremond, E.M.; Doughty, C.L.; Williams, A.P.; Parker, J.D.; Hayes, M.A.; Rodriguez, W.; Feller, I.C. Climate-Driven Regime Shifts in a Mangrove-Salt Marsh Ecotone Over the Past 250 Years. *Proc. Natl. Acad. Sci. USA* **2019**, *116*, 21602–21608. [CrossRef] [PubMed]

17. Rodriquez, E.; Cohen, M.C.L.; Liu, K.; Pessenda, L.C.R.; Yao, Q.; Ryu, J.; Rossetti, D.; de Souza, A.; Dietz, M. The Effect of Global Warming on the Establishment of Mangroves in Coastal Louisiana during the Holocene. *Geomorphology* **2021**, *381*, 107648. [CrossRef]

18. Yao, Q.; Liu, K. Dynamics of Marsh-Mangrove Ecotone Since the mid-Holocene: A Palynological Study of Mangrove Enroachment and Sea Level Rise in the Shark River Estuary, Florida. *PLoS ONE* **2017**, *12*, e0173670. [CrossRef]

19. United States Fish and Wildlife Service. *South Florida Multi-Species Recovery Plan*; U.S. Fish and Wildlife Service: Atlanta, GA, USA, 1999. Available online: https://www.nrc.gov/docs/ML1219/ML12193A340.pdf (accessed on 20 September 2021).

20. Smee, D.L.; Sanchez, J.A.; Diskin, M.A.; Trettin, C. Mangrove Expansion into Salt Marshes Alters Associated Faunal Communities. *Estuar. Coast. Shelf Sci.* **2017**, *187*, 306–313. [CrossRef]

21. Kelleway, J.J.; Cavanaugh, K.; Rogers, K.; Feller, I.C.; Ens, E.; Doughty, C.; Saintilan, N. Review of the Ecosystem Service Implications of Mangrove Encroachment into Salt Marshes. *Glob. Chang. Biol.* **2017**, *23*, 3967–3983. [CrossRef]

22. Vaughn, D.R.; Bianchi, T.S.; Shields, M.R.; Kenney, W.F.; Osborne, T.Z. Increased Organic Carbon Burial in Northern Florida Mangrove-Salt Marsh Transitional Zones. *Glob. Biogeochem. Cycles* **2020**, *34*, e2019GB006334. [CrossRef]

23. Cahoon, D.R.; McKee, K.L.; Morris, J.T. How Plants Influence Resilience of Salt Marsh and Mangrove Wetlands to Sea-Level Rise. *Estuaries Coast* **2021**, *44*, 883–898. [CrossRef]

24. Chmura, G.L.; Aharon, P. Stable Carbon Isotope Signatures of Sedimentary Carbon in Coastal Wetlands as Indicators of Salinity Regime. *J. Coast. Res.* **1995**, *11*, 124–135.

25. Wilson, K.R.; Kelley, J.T.; Tanner, B.R.; Belknap, D.F. Examining North-Temperate Salt-Marsh Geologic Records: Determining Origin of and Defining a Unique Stratigraphic Signature for Salt Pools of Six Maine Salt Marshes, U.S.A. *J. Coast. Res.* **2010**, *26*, 1007–1026. [CrossRef]

26. Khan, N.S.; Vane, C.H.; Horton, B.P. Stable Carbon Isotope and C/N Geochemistry of Coastal Wetland Sediments as a Sea-level Indicator. In *Handbook of Sea-Level Research*, 1st ed.; Shennan, I., Long, A.J., Horton, B.P., Eds.; John Wiley & Sons: New York City, NY, USA, 2015; pp. 295–311.

27. Tanner, B.R.; Douglas, M.L.; Greenberg, C.H.; Chamberlin, J.N.; Styers, D.M. A Macroscopic Charcoal and Multiproxy Record From Peat Recovered from Depression Marshes in Longleaf Pine Sandhills, Florida, USA. *Quaternary* **2018**, *1*, 25. [CrossRef]

28. Waller, S.S.; Lewis, J.K. Occurrence of C3 and C4 Photosynthetic Pathways in North American Grasses. *J. Range Manag.* **1979**, *32*, 12–28. [CrossRef]

29. Cerling, T.E.; Quade, J.; Wang, Y.; Bowman, J.R. Carbon Isotopes in Soil and Paleosols as Ecologic and Paleoecologic Indicators. *Nature* **1989**, *341*, 138–139. [CrossRef]

30. FNAI—Florida Natural Areas Inventory. *Guide to the Natural Communities of Florida: 2010 Edition*; Florida Natural Areas Inventory: Tallahassee, FL, USA, 2010; 276p. Available online: https://www.fnai.org/species-communities/natcom-guide (accessed on 20 September 2021).

31. Brady, N.; Weil, R. *Elements of the Nature and Properties of Soils*, 2nd ed.; Prentice Hall: Upper Saddle River, NJ, USA, 2003; 624p.

32. Reimer, P.J. IntCal13 and Marine13 Radiocarbon Age Calibration Curves, 0–50,000 Years Cal BP. *Radiocarbon* **2013**, *55*, 1869–1887. [CrossRef]

33. França, M.C.; Pessenda, L.C.R.; Cohen, M.C.L.; de Azevedo, A.Q.; Fontes, N.A.; Silva, F.B.; de Melo, J.C.F., Jr.; Piccolo, M.C.; Bendassolli, J.A.; Macario, K. Late-Holocene Subtropical Mangrove Dynamics in Response to Climate Change During the Last Millennium. *Holocene* **2019**, *29*, 445–456. [CrossRef]

34. Harrison, A.F.; Bocock, K.L. Estimation of Soil Bulk Density from Loss-On-Ignition Values. *J. Appl. Ecol.* **1981**, *8*, 919–927. [CrossRef]

35. Hatté, C.; Jull, A.J. Radiocarbon Dating: Plant Macrofossils. *Encycl. Quat. Sci.* **2007**, 2958–2965. [CrossRef]

36. Sefton, J.; Woodroffe, S.; Ascough, P. Radiocarbon Dating of Mangrove Sediments. In *Dynamic Sedimentary Environments of Mangrove Coasts*; Sidik, F., Friess, D.A., Eds.; Elsevier: Amsterdam, The Netherlands, 2021; pp. 199–215.

37. Alongi, D.M. Carbon Cycling and Storage in Mangrove Forests. *Annu. Rev. Mar. Sci.* **2014**, *6*, 195–215. [CrossRef]

38. Goñi, M.A.; Thomas, K.A. Sources and Transformations of Organic Matter in Surface Soils and Sediments from a Tidal Estuary (North Inlet, South Carolina, USA). *Estuaries* **2000**, *23*, 548–564. [CrossRef]

39. Drexler, J.Z.; Davis, M.J.; Woo, I.; De La Cruz, S. Carbon Sources in the Sediments of a Restoring vs. Historically Unaltered Salt Marsh. *Estuaries Coasts* **2020**, *43*, 1345–1360. [CrossRef]

40. Schuerch, M.; Dolch, T.; Bisgwa, J.; Vafeidis, A.T. Changing Sediment Dynamics of a Mature Backbarrier Salt Marsh in Response to Sea-Level Rise and Storm Events. *Front. Mar. Sci.* **2018**, *5*, 155. [CrossRef]

41. Mcleod, E.; Chmura, G.L.; Bouillon, S.; Salm, R.; Björk, M.; Duarte, C.M.; Lovelock, C.; Schlesinger, W.H.; Silliman, B.R. A blueprint for blue carbon: Toward an improved understanding of the role of vegetated coastal habitats in sequestering CO_2. *Front. Ecol. Environ.* **2011**, *9*, 552–560. [CrossRef]